Sciencexpress Report

Entangled Macroscopic Quantum States in Two Superconducting Qubits

A. J. Berkley,* H. Xu, R. C. Ramos, M. A. Gubrud, F. W. Strauch, P. R. Johnson, J. R. Anderson, A. J. Dragt, C. J. Lobb, F. C. Wellstood

Center for Superconductivity Research, Department of Physics, University of Maryland, College Park, MD 20742, USA.

*To whom correspondence should be addressed. E-mail: berkley@physics.umd.edu

We present spectroscopic evidence for the creation of entangled macroscopic quantum states in two current-biased Josephson-junction qubits coupled by a capacitor. The individual junction bias currents are used to control the interaction between the qubits by tuning the energy level spacings of the junctions in and out of resonance with each other. Microwave spectroscopy in the 4-6 GHz range at 20 mK reveals energy levels which agree well with theoretical results for entangled states. The single qubits are spatially separate and the entangled states extend over the 0.7 mm distance between the two qubits.

Most research on quantum computation (*1*) using solid-state systems has been focused on the behavior of single isolated quantum bits (qubits) (*2*–*9*). For example, progress in the last two years on single superconducting qubits has included the observation and control of states formed from quantum superpositions (*3*–*9*). In addition to quantum superpositions, quantum computation also requires the entanglement of multiple qubits (*10*). Entanglement is critical for enabling a quantum computer to be exponentially faster than a classical one (*11*) and means that the state of one qubit depends inextricably on the state of another qubit. Recently, entanglement in a superconducting charge-based two-qubit system with an overall size of a few micrometers has been reported (*3*). We describe a different superconducting coupled qubit system with qubits separated by a distance that is hundreds of times larger. Our microwave spectroscopic measurements (*12*, *13*] show clear evidence for entangled states in this macroscopic system.

Each of our qubits is formed by a single current-biased Josephson junction (*14*). The behavior of such a junction is analogous to a particle of mass C_j that moves in a tilted washboard potential (Fig. 1A) (*15*):

$$U(\gamma) = -I_c\,(\Phi_0/2\pi)\cos(\gamma) - I_b\,\gamma\Phi_0/2\pi \qquad (1)$$

where I_b is the bias current flowing through the junction, I_c is the critical current, C_j is the junction capacitance, $\Phi_0 = 2.07 \times 10^{-15}$ T-m^2 is the flux quantum, and γ is the phase difference of the quantum mechanical wavefunction across the junction (*15*). We note that γ is a collective degree of freedom for the roughly 10^9 paired electrons in the metal from which the qubit is constructed (*16*) and $d\gamma/dt$ is proportional to the voltage across the junction. Quantization of this system leads to metastable states which are localized in the potential well and have well-defined energies (Fig. 1A). The lifetimes of the states can be long, provided an appropriate isolation network prevents the junction from dissipating energy to its bias leads (*2*, *4*, *5*, *12*,*13*). At bias currents I_b slightly lower than I_c there are only a few states trapped in the well, and the barrier is low enough to allow escape by quantum tunneling (*17*, *18*) to a set of continuum states which exhibit an easily detectable DC voltage.

We couple two junction qubits together by using a capacitor C_c (Fig. 1B) (*19*–*21*). The strength of the qubit-qubit coupling is set by $C_c/(C_j+C_c)$, which for our qubits is about 0.1. When the current through one qubit is adjusted to produce an energy level spacing equal to that in the other qubit, the capacitive coupling leads to mixing of the uncoupled states and a lifting of the energy degeneracy (*19*). Near this "equal-spacing" bias point the three lowest levels of the system are the ground state $|00\rangle$, and two excited states $(|01\rangle \pm |10\rangle)/\sqrt{2}$. Here the notation $|01\rangle$ indicates, for example, that the first qubit is in its ground state $|0\rangle$ and the second is in its first excited state $|1\rangle$. We note that these two-qubit excited states are entangled; when qubit 1 is found in the ground state $|0\rangle$, then qubit 2 is found in the excited state $|1\rangle$ and vice versa.

Our qubits are fabricated using a Nb-AlO_x-Nb thin film trilayer process on 5 mm × 5 mm Si chips (Fig. 1C). Each qubit is a 10 μm×10 μm Josephson junction. The coupling is created by two 60 μm×60 μm Nb-SiO_2-Nb thin film capacitors, and the separation between the two qubits is 0.7 mm. To observe the states of the system, we cool the chip to 20 mK in a dilution refrigerator, thereby reducing thermal excitations and allowing the junction to relax to the ground state. The current bias lines to each junction are carefully filtered; in addition, on-chip LC filters are used to reduce dissipation from the bias lines (*12*). We use a magnetic field of a few mT applied in the plane of the junctions to tune their critical currents to around 15 μA, which gives an energy level spacing in the 5-10 GHz range.

We perform spectroscopy on the coupled qubit system by applying microwave power through the bias lines to induce transitions from the ground state to high energy states. As the higher energy states have faster tunneling rates, this results in an enhancement of the rate at which the system tunnels to the DC voltage state. For the measurements shown in Fig. 2, we set the bias current of qubit 1 at I_{b1} = 14.630 μA (just below the critical current), apply steady microwave power, and slowly ramp the bias current I_{b2} of qubit 2 while waiting for a junction escape event. We record the bias current I_{b2} at which either junction escapes and repeat the ramping process up to 10^5 times to obtain a histogram of escape events as a function of I_{b2}. By using the current ramp rate and the amount of time spent in each histogram bin, we calculate the escape rate as a function of I_{b2} (*12*). As expected, a well-defined Lorentzian peak in the escape rate appears at currents where the transition frequency from the ground state to an excited state equals the microwave drive frequency (Fig. 2A). We track these peak locations as a function of drive frequency, thereby obtaining the spectrum of allowed transitions (see open circles in Fig. 2B).

Examination of Fig. 2B shows that for each value of I_{b2}, there are two transitions out of the ground state (a lower level from 4.5 to 4.95 GHz and an upper level from 5.2 to 5.9 GHz, depending on I_{b2}), and an apparent gap from 4.9 to 5.2 GHz. This behavior is characteristic of an avoided level crossing. Repeating the measurement at different I_{b1} or I_c (tuned by an applied magnetic field) moves the gap up and down in the expected manner; lower I_{b1} or a larger I_c increases the energy level spacing in qubit 1 and pushes the gap to higher frequencies. As a check, we have also measured single uncoupled qubits which, as expected, do not show this avoided crossing. In addition, when more microwave power is applied, we observe multi-photon transitions to higher levels (*22*) as well as transitions from thermally populated excited states (*12*) which are also expected from the quantum mechanical behavior of the system.

To verify that the transitions observed in Fig. 2B are due to the entangled states, we compare our results to the expected splitting calculated from quantum mechanics using independently measured parameters of each qubit. Analysis of the coupled qubit circuit reveals that the Hamiltonian for the system is (*19*):

$$H = \frac{p_1^2}{2m} - \frac{\Phi_0}{2\pi}\left(I_{c1}\cos(\gamma_1) + I_{b1}\gamma_1\right) + \frac{p_2^2}{2m} - \frac{\Phi_0}{2\pi}\left(I_{c2}\cos(\gamma_2) + I_{b2}\gamma_2\right) + \frac{\zeta}{m}p_1 p_2 \quad (2)$$

with $m = C_j(1+\zeta)(\Phi_0/2\pi)^2$, $\zeta = C_c / (C_c + C_j)$,

$p_1 = (C_c + C_j)\left(\frac{\Phi_0}{2\pi}\right)^2(\dot{\gamma}_1 - \zeta\dot{\gamma}_2)$, and

$p_2 = (C_c + C_j)\left(\frac{\Phi_0}{2\pi}\right)^2(\dot{\gamma}_2 - \zeta\dot{\gamma}_1)$. The momenta, p_i, are roughly proportional to the voltage on the i^{th} qubit and result from the stored energy on the junction and coupling capacitors (*19*).

To obtain the qubit parameters, we repeat the spectroscopic measurements with I_{b1} set to zero. This increases the energy level spacing in qubit 1, and the location of the gap in the spectrum, to greater than 15 GHz. In this situation, although the two qubits are still physically coupled, the levels probed by our low measuring frequency (4 to 6 GHz) are approximately the uncoupled energy levels of qubit 2 (black squares in Fig. 2B). We fit this spectrum to a numerical solution of the Schrödinger equation for the Hamiltonian in Eq. 2 (Fig. 2B, black dashed line) with I_{b1}=0 to obtain I_{c2} = 15.421 ±0.002 μA and $(1+\zeta)C_j$ = 5.63 ±0.07 pF. In an analogous manner, we measure the energy level spacing for qubit 1 (black cross in Fig. 2b) when it is decoupled from qubit 2 and obtain I_{c1} = 14.779 ±0.004 μA. We fit the avoided level crossing data (white circles in Fig. 2b) by varying C_c, C_j and I_{c1} around their measured values, finding $C_c \approx 0.7$ pF, $C_j \approx 4.8$ pF, and $I_{c1} \approx 14.778$ μA. The coupling capacitance compares favorably with the design value $C_c \approx 0.8$ pF, and the fitted values of I_{c1} and C_j are consistent with the independent measurements. The resulting fit, given by the solid white curves in Fig. 2B, shows excellent agreement with the data, strongly supporting the existence of entangled states of the system.

Our spectroscopic measurements can be used to show that the system is quantum mechanical and not classical. We note that there is no classical analog to discrete transitions between higher levels ($|1\rangle \rightarrow |2\rangle$ and above) nor to quantum tunneling, which is directly visible as a saturation in the escape rate as the temperature is lowered. We also do not see classical anharmonic oscillator effects (*23*) such as a significantly non-Lorentzian resonance line shape at large powers or a shift to lower resonance frequency with increased drive power. Finally, classical theory predicts resonance frequencies that are significantly higher than the quantum transition frequencies we observe. This consistency with quantum theory and inconsistency with classical theory makes a classical explanation for the avoided crossing implausible.

Our spectroscopic measurements can also be used to determine the coherence time, τ_c, of the states by measuring the width of the transition in current and converting to a width in frequency using the measured dependence of the transition frequency on the currents. For the decoupled situation, the $|00\rangle \rightarrow |01\rangle$ transition has $\tau_c \approx 2$ ns, consistent with decoherence caused by low-frequency current noise in the bias lines (*24*). For the coupled situation, the $|00\rangle \rightarrow (|01\rangle \pm |10\rangle)/\sqrt{2}$ transitions have $\tau_c \approx 2$ ns as well.

While these spectroscopic coherence times are shorter than desirable for quantum computation, it is encouraging that the entangled states do not decohere noticeably faster than the uncoupled states. This is remarkable considering the large number of paired electrons involved, the presence of bias leads, and the expectation that spatially extended entangled states would be very susceptible to decoherence. Such evidence for entanglement over a macroscopic length is particularly promising for construction of a quantum computer, as this will require many spatially separated qubits. Better isolation schemes (*4*, *5*) and pulsed microwave or other gate methods (*25*) should allow demonstrations of Rabi oscillations and ultimately Bell inequality violations of these entangled states, as well as lead to the longer coherence times needed for actual computation.

References

1. R. Hughes *et al.*, *A quantum information science and technology roadmap.* (2002, http://qist.lanl.gov).
2. R. C. Ramos *et al.*, *IEEE Trans. Appl. Supr.* **11**, 998 (2001).
3. Y. A. Pashkin *et al.*, *Nature* **421**, 823 (2003).
4. J. M. Martinis, S. Nam, J. Aumentado, C. Urbina, *Phys. Rev. Lett.* **89**, 117901 (2002).
5. Y. Yu, S. Han, X. Chu, S. Chu, Z. Wang, *Science* **296**, 886 (2002).
6. Y. Nakamura, Y. Pashkin, J. S. Tsai, *Nature* **398**, 786 (1999).
7. D. A. Vion *et al.*, *Science* **296**, 886 (2002).
8. J. R. Friedman, V. Patel, W. Chen, S. K. Tolpygo, J. E. Lukens, *Nature* **406**, 43 (2000).
9. C. H. van der Wal *et al.*, *Science* **290**, 773 (2000).
10. M. A. Nielsen, I. L. Chuang, *Quantum Computation and Quantum Information* (Cambridge Univ. Press, Cambridge, 2001).
11. R. Jozsa, N. Linden (quant-ph/0201143).
12. A. J. Berkley *et al.*, *IEEE Trans. Appl. Supr.*, **13** (2003). in press.

13. J. M. Martinis, M. H. Devoret, J. Clarke, *Phys. Rev. Lett.* **55**, 1543 (1985).
14. B. D. Josephson, *Phys. Lett.* **1**, 251 (1962).
15. see eg. M. Tinkham, *Introduction to Superconductivity* (McGraw Hill, New York, 1996), second edn.
16. A. J. Leggett, *Suppl. Prog. Theor. Phys.* **69**, 80 (1980).
17. R. F. Voss, R. A. Webb, *Phys. Rev. Lett.* **47**, 265 (1981).
18. M. H. Devoret, J. M. Martinis, J. Clarke, *Phys. Rev. Lett.* **55**, 1908 (1985).
19. P. R. Johnson *et al.*, *Phys. Rev. B* **67**, 020509 (2003).
20. A. Blais, A. Maassen van den Brink, A. M. Zagoskin, *Phys. Rev. Lett.*, **90**, 127901 (2003).
21. R. C. Ramos *et al.*, *IEEE Trans. Appl. Supr.*, **13** (2003). in press.
22. A. Wallraff, T. Duty, A. Lukashenko, A. V. Ustinov, *Phys. Rev. Lett.* **90**, 037003 (2003).
23. see eg. L. D. Landau, E. M. Lifshitz, Mechanics (Butterworth-Heinemann, Oxford, 1976), third edn.
24. A. J. Berkley *et al.* . (quant-ph/0303001).
25. F. W. Strauch *et al.* (quant-ph/0303002).
26. We acknowledge support from DOD and the Center for Superconductivity Research. Hypres Inc. fabricated the niobium samples. We thank R. Webb for many useful discussions.

14 March 2003; accepted 30 April 2003

Published online 15 May 2003;
<zdoi;10.1126/science.1084528>

Include this information when citing this paper.

Fig. 1. Josephson junction qubits. A. Potential energy of single qubit with two energy levels depicted. The solid vertical arrow represents the action of the microwave drive while the horizontal dashed arrow shows the quantum tunneling escape mechanism. B. Schematic of two coupled qubits. Qubits are coupled by capacitance C_c, and biased individually with a linear ramp on qubit 2 and a DC bias on qubit 1. Microwave current I_m is applied to qubit 2 through the bias line. Estimated parameters are: I_{c2} = 15.421 μA, C_j=4.8 pF, C_c=0.7 pF (giving ζ = 0.13), I_{b1} = 14.630 μA, I_{c1} = 14.779 μA. C. Photo of two coupled qubits. The lower coupling capacitor is present to short out parasitic inductance in the ground line, and together with the upper coupling capacitor forms C_c. Spiral inductors lead to bias lines. There is no on-chip ground plane, it is provided by the copper box the chip is mounted in. D. Photo of 10 μm×10 μm Nb-AlO_x-Nb Josephson junction.

Fig. 2. Spectroscopy on coupled qubits showing avoided level crossing. A. Measured resonance enhancement peak for $|00\rangle \rightarrow (|01\rangle - |10\rangle)/\sqrt{2}$ transition measured for microwave power applied at f=4.7 GHz. $\Delta = (\Gamma_m - \Gamma)/\Gamma$ is plotted vs. I_{b2}, where Γ is the escape rate without microwaves and Γ_m is the escape rate with microwaves. B. Color plot of normalized Δ as a function of microwave drive frequency (y-axis) and bias current I_{b2} through qubit 2 (x-axis). Each data set (horizontal stripe, as in (A) above) is normalized so the highest peak is unity (red), with green signifying zero, and blue negative enhancement. For each frequency, we adjust the microwave power so $\Delta < 5$ for all currents. Open circles mark centers of resonance peaks. Solid white lines are from theoretical calculation using parameters in Fig. 1. For comparison, decoupled $|0\rangle \rightarrow |1\rangle$ energy spacing for qubit 1 is shown by the dashed horizontal black line and cross while qubit 2 is the dashed diagonal black line and squares.

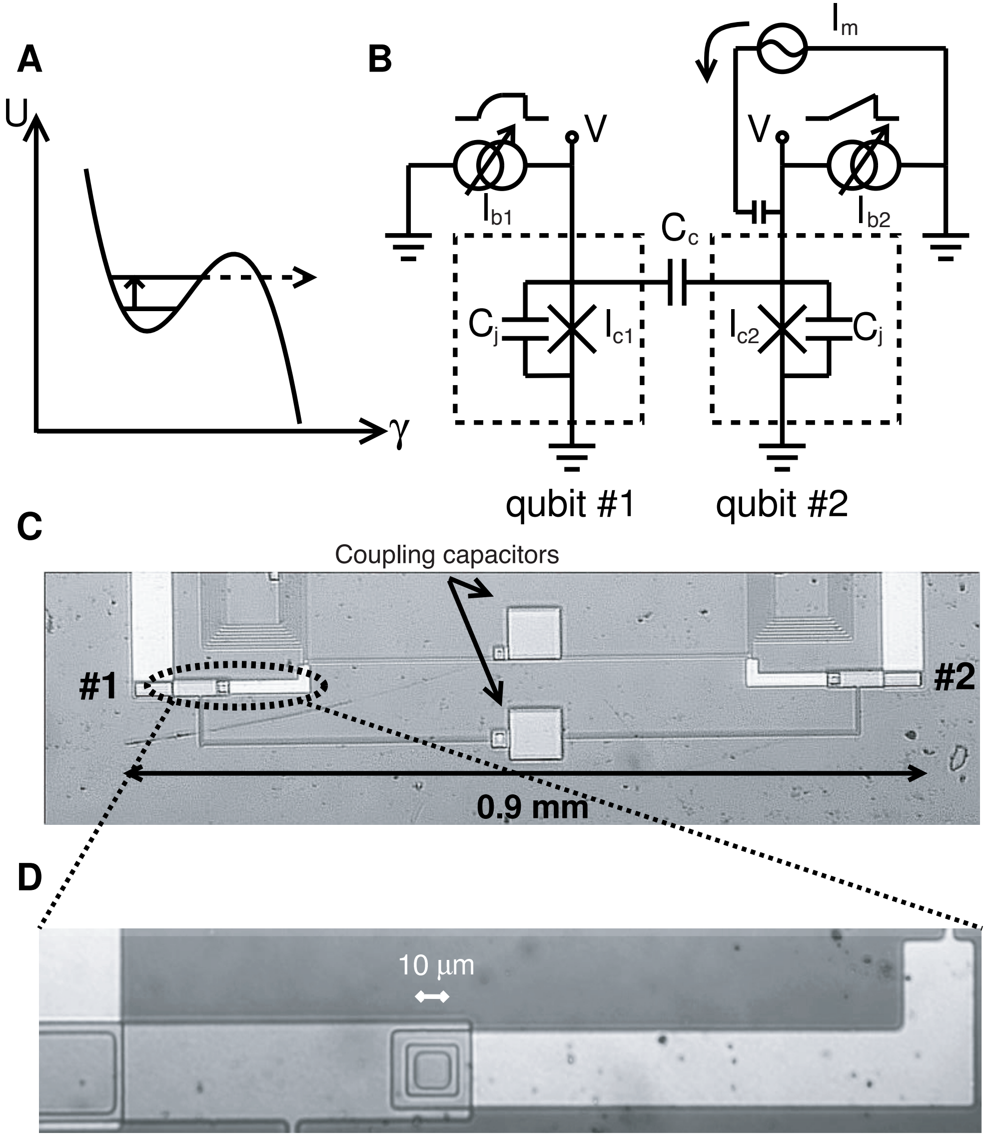
A
U
γ
B
I_m
V
V
I_{b1}
I_{b2}
C_c
C_j
I_{c1}
I_{c2}
C_j
qubit #1
qubit #2
C
Coupling capacitors
#1
#2
0.9 mm
D
10 μm

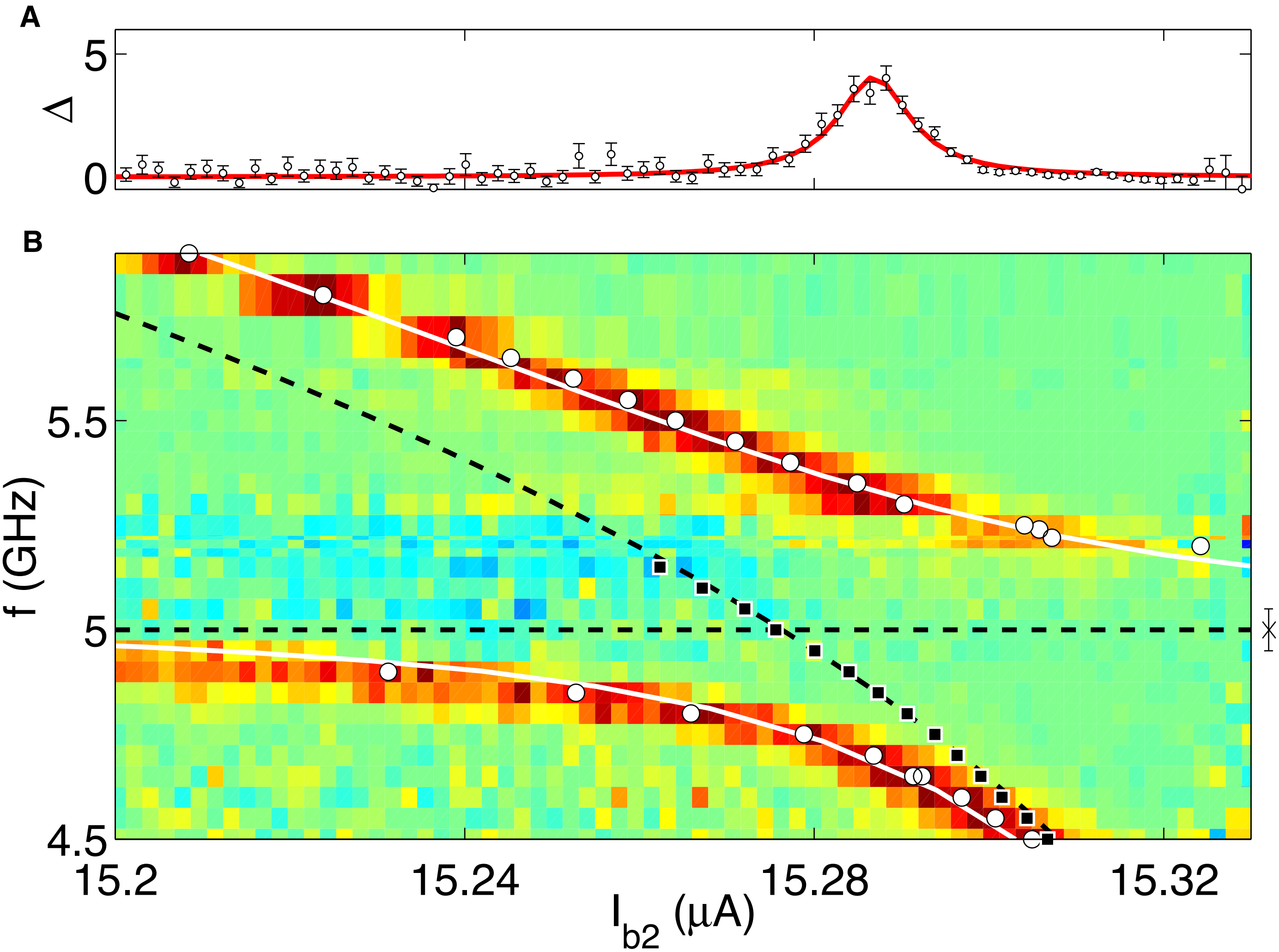

A
5
0
Δ
B
5.5
5
4.5
f (GHz)
15.2
15.24
15.28
15.32
I_{b2} (μA)